AIP Journal of Applied Physics

# Utility of reactively sputtered CuNx films in spintronics devices

Yeyu Fang, J. Persson, C. Zha, J. Willman, Casey W. Miller et al.

Citation: J. Appl. Phys. **111**, 073912 (2012); doi: 10.1063/1.3703067
View online: http://dx.doi.org/10.1063/1.3703067
View Table of Contents: http://jap.aip.org/resource/1/JAPIAU/v111/i7
Published by the American Institute of Physics.

## Related Articles



## Additional information on J. Appl. Phys.

JOURNAL OF APPLIED PHYSICS **111**, 073912 (2012)

# Utility of reactively sputtered $CuN_x$ films in spintronics devices

Yeyu Fang,[1] J. Persson,[1,2] C. Zha,[3] J. Willman,[4] Casey W. Miller,[4,a)] and Johan Åkerman[1,2,3,b)]

[1]*Physics Department, Göteborg University, 412 96 Göteborg, Sweden*
[2]*NanOsc AB, Electrum 205, 164 40 Kista, Sweden*
[3]*Materials Physics Department, Royal Institute of Technology, Electrum 229, 164 40 Kista, Sweden*
[4]*Department of Physics, Center for Integrated Functional Materials, University of South Florida, 4202 East Fowler Avenue, Tampa, Florida 33620, USA*

(Received 13 December 2011; accepted 11 March 2012; published online 13 April 2012)

We have studied nitrified copper ($CuN_x$) thin films grown by reactive sputtering in the context of spintronic devices. The Ar-to-$N_2$ flow ratio enables tunability of the electrical resistivity and surface roughness of the $CuN_x$ films, with the former increasing to nearly 20 times that of Cu, and the latter reduced to the atomic scale. Incorporating this into a Ta/$CuN_x$/Ta seed stack for spin valves improves the current-in-plane (CIP) magnetoresistance; maximum magnetoresistance results with $CuN_x$ seed layer and Cu interlayer. Finally, finite element modeling results are presented that suggest the use of $CuN_x$ in nanocontact spin torque oscillators can enhance current densities by limiting the current spread through the device. This may positively impact threshold currents, power requirements, and device reliability. © *2012 American Institute of Physics*. [http://dx.doi.org/10.1063/1.3703067]

## I. INTRODUCTION

Spintronic devices, based on scientific breakthroughs, such as giant magnetoresistive (GMR) (Refs. 1 and 2) and tunneling magnetoresistive (TMR) (Refs. 3–5), are, e.g., used in hard-drive read heads and magnetoresistive random access memory (MRAM).[6,7] The more recent effect of spin transfer torque (STT) (Refs. 8–10, 11) can also be used to induce microwave oscillations in both GMR (Refs. 12–14) and TMR (Refs. 15–17) elements, essentially creating a new class of microwave generators, so called spin torque oscillators (STOs). Typically, nanocontact based STOs (Ref. 18) offer the highest frequencies,[19] the widest frequency ranges, the fastest modulation rates,[20] the highest spectral purity,[21] and well defined spin wave modes.[22] With diameters of the order 100 nm, nanocontacts inject very high current densities (e.g., $\sim 10^8\,\mathrm{A/cm^2}$) into a pseudo spin valve mesa wherein the current becomes sufficiently spin polarized to excite ferromagnetic resonance (FMR) in one or both of the ferromagnetic layers. The resonance frequency can be tuned by the current density, i.e., the smaller the nano contact area, the steeper the current dependence of the STO frequency.[23]

Reducing the interface roughness in the mesa is important for maximizing the spin torque efficiency and GMR, minimizing damping caused by Néel coupling between the magnetic layers, and lowering the STO threshold current. Appropriate seed layers to promote the smoothest possible growth of all subsequent layers in the devices are hence of critical importance.

While typically overlooked, the resistivity of both seed and spacer layers plays a crucial role in nanocontact STOs. When the current enters the mesa through the nanocontact it will spread out laterally and reduce the current density in the subsequent magnetic layers. This greatly increases the total current needed for STO operation. If the current spread could be limited, e.g., by increasing the resistivity of the spacer layer, both the STO threshold current and the current required to reach high frequencies could be reduced, hence saving power, reducing heating, and leading to greater reliability of these devices. Here, we show that $CuN_x$ films have electrical resistivity and surface roughness that can be tailored by nitrogen content, making them potentially useful in a variety of spintronics devices.[24,25] We combine Cu and $CuN_x$ seed and spacer layers and demonstrate all four types of spin valves with GMR properties governed by both roughness and resistivity. We finally present simulations of nanocontact STOs, where the utility of a spacer layer with high resistivity and seed layer with low resistivity is clearly demonstrated as it controls the lateral spreading of the current in the device.

## II. EXPERIMENTAL

Ta (5 nm)/$CuN_x$(20 nm)/Ta(5 nm) trilayers were rf sputtered onto natively oxidized silicon (100) substrates at room temperature. The base pressure of the system was better than $5 \times 10^{-8}$ Torr. Ta layers were deposited at 150 W in 5 mTorr of Ar flowing at 25 sccm. The $CuN_x$ layers were grown by rf reactive sputtering from a Cu target in a variety of Ar-$N_2$ mixtures held at 5.0 mTorr. A constant total gas flow of 25 sccm was achieved by independently controlling the Ar and $N_2$ flow rates, $\dot{A}r$ and $\dot{N}_2$, respectively. The N-content in the films was controllable via the fractional $N_2$ flow, $F = \dot{N}_2/25$ sccm. In addition, $CuN_x$ samples were grown with a 5 W rf bias applied during deposition. After deposition, the room temperature resistivity was deduced from sheet resistance measurements using four-point probe techniques, the surface roughness was measured by atomic force microscopy (AFM), and the structural properties were investigated by X-ray diffraction (XRD) and X-ray reflectivity (XRR) with Cu $K_\alpha$ radiation.

a)Electronic mail: millercw@usf.edu.
b)Electronic mail: akerman1@kth.se.

 

## III. RESULTS AND DISCUSSION

The XRD patterns for seed stacks demonstrate a structural evolution with increasing F (Fig. 1). For brevity, only the rf biased sample scans are shown here. Biasing tends to enhance the diffraction peak's shape, presumably by providing some level of strain relief, but had no other observed impact in the high angle diffraction. The pronounced Cu(111) peak decreases with F until it disappears above 5% nitrogen flow. At F = 3%, Cu(200) texture appears abruptly, coexisting with Cu(111). At this point the surface roughness is dramatically reduced, as shown in Fig. 2. The Cu(200) intensity increases with F at the same time as Cu(111) intensity and surface roughness further decreases. Only the Cu(200) peak exists for F of 10%, which corresponds to the surface roughness minimum. A $Cu_3N$ (200) peak appears for F between 10% and 20%, coexisting with the Cu(200) peak until 30%, above which the former is dominant. Thus, the presence of Cu(200) texture is strongly correlated with minimizing the surface roughness; coexistence of either Cu(111) or $Cu_3N$ leads to increased roughness.

The surface roughness is also tunable through F, as shown in Fig. 2. While the pure Cu-based seed stack has the largest roughness (~7.5–8 Å), small amounts of nitrogen cause the roughness to be dramatically reduced, irrespective of substrate biasing. The roughness is minimized to 2.7 Å for F = 10%, above which it gradually increases. The smooth trend of roughness with F implies that rf biasing seems to enable a more reproducible sample preparation.

Figure 3 shows X-ray reflectivity data for both deposition sets. Because X-rays penetrate the sample, we obtain a different perspective on the structure than from AFM measurements. In each trace, the high frequency oscillations correspond to the thicker $CuN_x$ layer, and the low frequency oscillations correspond to the Ta layers. As with the AFM data, a clear shift in roughness is detected at F = 3% when rf biasing is used, as evidenced by the $CuN_x$-based oscillations persisting to higher values of Q. Without biasing, the structure is improved for F

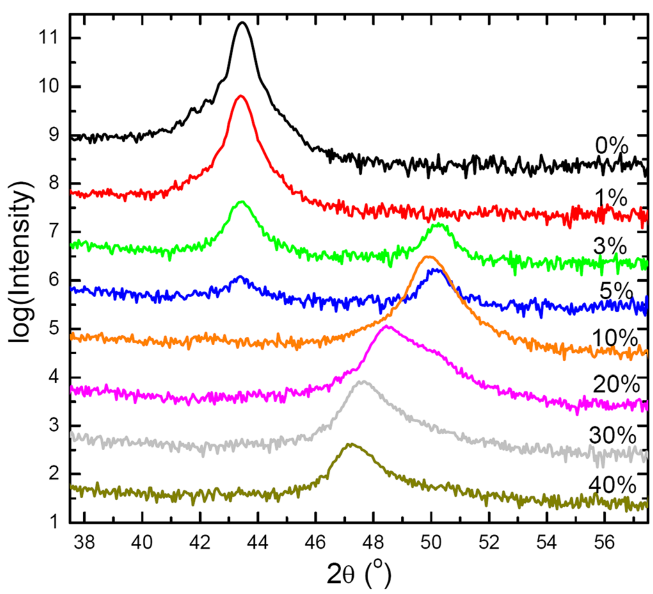


FIG. 1. X-ray diffraction measurements reveal a transition from Cu(111) to Cu(200) and $Cu_3N$(200) with increasing nitrogen fraction. The roughness is minimized for 10% $N_2$, where the Cu(200) texture dominates.

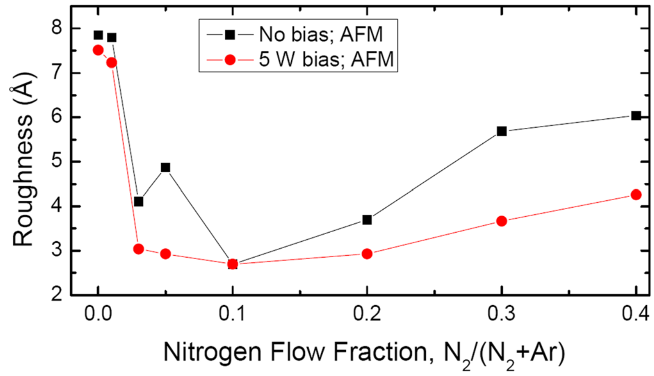


FIG. 2. The dependence of the roughness of Ta/$CuN_x$/Ta trilayers on the fractional flow of $N_2$ in the mixed $N_2$ + Ar gas with and without 5 W rf biasing during deposition. Atomic force microscopy results are for the top surface only. The lines are guides to the eye.

between 10% and 30%. The surface roughness for the top Ta layer obtained from fitting XRR data using the Parratt formalism is 2.9 Å, and is in reasonable agreement with the AFM measurement of 2.7 Å. The nominal layer thicknesses, which were estimated by independently calibrated sputtering rates and computer controlled deposition times, are consistent with

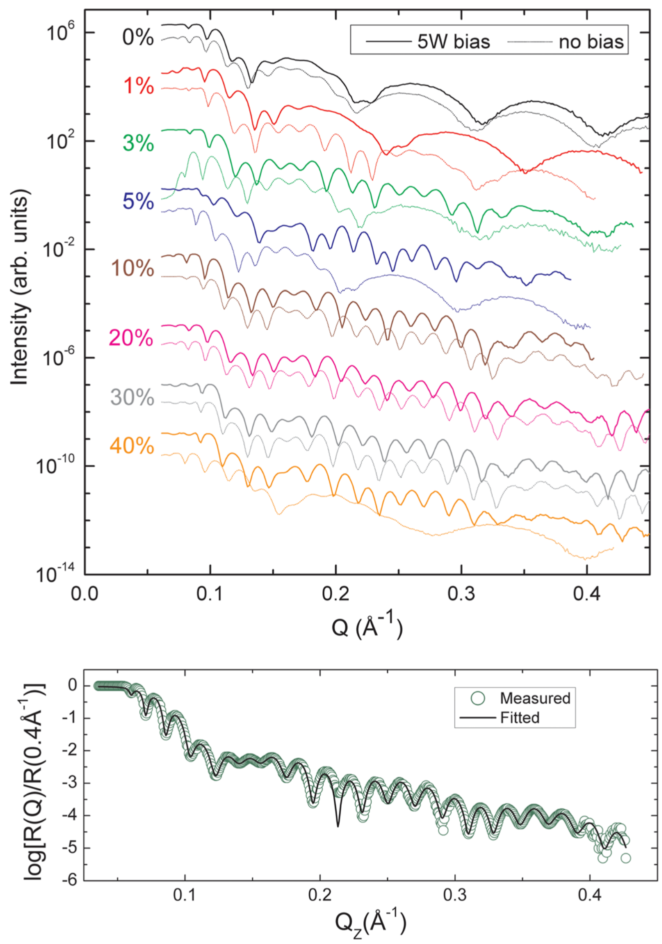


FIG. 3. X-ray reflectivity measurements for Ta/$CuN_x$/Ta trilayers with the noted $N_2$ fraction during the Cu sputtering with and without rf biasing during the deposition. Biasing helps to reduce the roughness at lower nitrogen fractions than is otherwise possible without biasing. The bottom panel shows the XRR data (circles) with the best fit (line) for the rf biased sample grown with F = 10%.

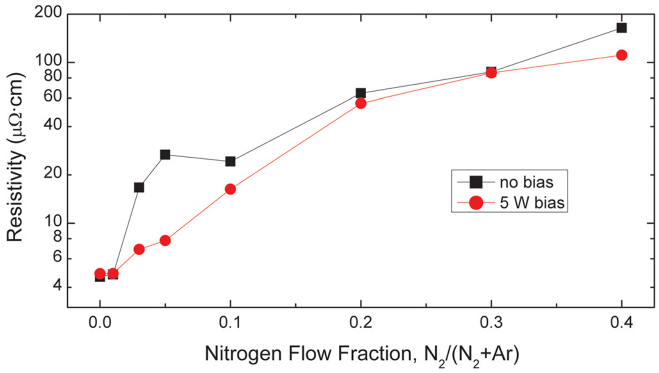


FIG. 4. The dependence of the electrical resistivity of $CuN_x$ in Ta/$CuN_x$/Ta trilayers on the fractional flow of $N_2$ in the mixed $N_2$ + Ar gas with and without 5 W rf biasing during deposition. The lines are guides to the eye.

the fitted values. Although the initial Ta seed layer has a significantly rough surface of 8.8 Å, the nitrified Cu layer reduces the roughness dramatically. This indicates that the nitrified Cu acts to planarize the structure, which ultimately reduces the interfacial roughness of subsequently deposited layers. It is well known that roughness is detrimental to magnetic devices through either the formation of tunneling "hot spots"[26,27] or "orange peel" coupling.[28,29] Thus, the incorporation of Cu-N into seed layer structures may improve performance of many technologically relevant applications.

The dependence of the $CuN_x$ resistivity on F is shown in Fig. 4 for samples deposited with and without rf substrate biasing. The $CuN_x$ resistivity was extracted from the Ta/$CuN_x$/Ta structure using a parallel resistor model, having separately measured the resistivity of 5 nm Ta to be 216 $\mu\Omega \cdot$ cm. The resistivity increased with $N_2$ flow fraction, and was more controllable with rf biasing. Since $Cu_3N$ has insulator properties,[24,25] this behavior is expected. With the partially nitrified Cu layer having higher resistivity than pure Cu, the total resistivity for the trilayer seed stack increases.

In addition to its incorporation in the seed stack, we investigated $CuN_x$ as the nonmagnetic interlayer in GMR spin valves (SVs) grown on seed stacks (Table I). The general structure was Ta (5 nm)/$CuN_x$ (20 nm)/Ta (5 nm)/CoFe (5 nm)/$CuN_x$ (6 nm)/NiFe (6 nm)/Ta (3 nm)/Pt (3 nm). An in-plane magnetic field was used during the deposition to define the easy axes of the ferromagnetic layers. Magnetoresistance (MR) measurements were made at room temperature using a four-point probe method. The current-in-plane (CIP) configuration was used with the field parallel to the current and the easy axis. Two preparations of $CuN_x$ were used: zero $N_2$ flow (i.e., pure copper), and 10% $N_2$ fraction (i.e., that which previously minimized roughness). This allowed us to investigate

TABLE I. Current-in-plane giant magnetoresistance results for four samples whose seed layer and spin-valve interlayer were sputtered with 0% and 10% nitrogen flow fraction.

| | | Seed layer | |
|---|---|---|---|
| | | 0% | 10% |
| Interlayer | 0% | 0.63% | 1.04% |
| | 10% | 0.15% | 0.38% |

four distinct SV combinations: of (0%, 0%), (10%, 0%), (0%, 10%), and (10%, 10%), where the ordered pair refers to the $N_2$ fraction in the (seed stack spacer, SV interlayer). Keeping the spin valve interlayer layer as pure Cu, the CIP-MR increases from 0.63% to 1.04% when the seed stack spacer is grown with 10% $N_2$ fraction. Similarly, when the spin valve interlayer layer is nitrified, the CIP-MR value increases when the seed stack spacer is nitrified, but from only 0.15% to 0.38%. Thus, the CIP-MR is maximized for (10%, 0%), and minimized for the (0%, 10%). Both of these make sense: (10%, 0%) has a smooth seed stack and high conductivity interlayer, while (0%, 10%) is rough with low conductivity interlayer.

While the increased resistivity of the $CuN_x$ films is apparently detrimental as a spacer layer in spin valves, it may be beneficial for spin transfer devices. In STOs, current is injected along the surface normal into a spin-valve-like structure from a nanocontact (e.g., 100 nm diameter), as depicted in Fig. 5(a). This multilayer is typically of much larger diameter than the nanocontact (e.g., 1 $\mu$m), which allows the current to spread out laterally as it travels into the spin valve, effectively increasing the diameter of the nanocontact. This is detrimental to

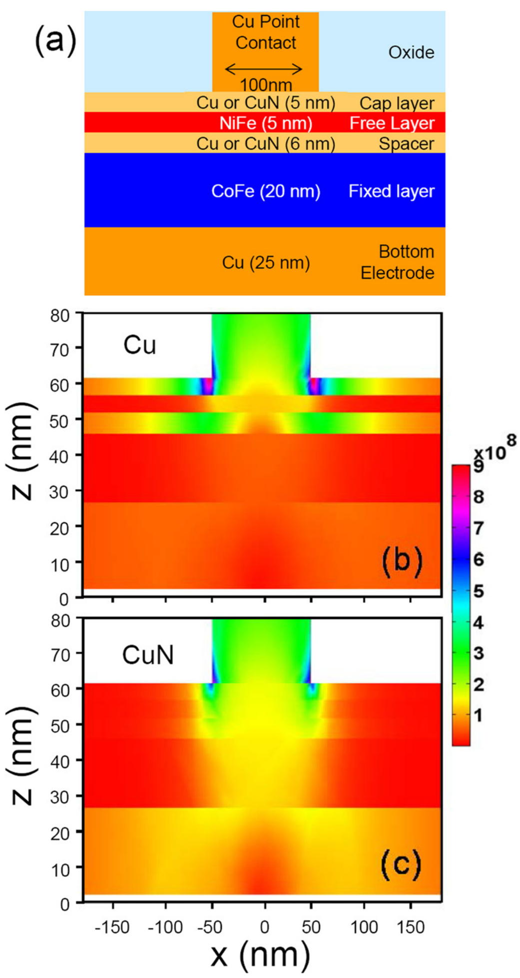


FIG. 5. (a) Schematic of the structure used in COMSOL simulations. The simulated current densities are greater in the cap and spacer layers of the Cu-based STO (b) than in the CuN-based STO (c), which reduces the current density in the free and fixed layers. The total current density is more uniform near the nanocontact in the $CuN_x$ device, and it clearly penetrates into the fixed layer before dissipating. The color bar has units of A/cm$^2$.

STOs because current density is an important parameter for spin transfer phenomena. The higher resistivity of nitrified Cu is thus worth exploring as a means to limit the amount of current spreading that takes place. This could enable a relative increase in the achievable current density in STOs.

We used finite element modeling (COMSOL software) to investigate the current density in STOs whose cap and spacer layers were both Cu or both $CuN_x$ (Fig. 5(a)). The structure investigated was Cu point-contact/[Cu or $CuN_x$](5 nm)/NiFe(5 nm)/[Cu or $CuN_x$](5 nm)/CoFe(20 nm)/Cu(25 nm). The diameter of the point-contact was 100 nm; the diameter of the underlying SV was 1 $\mu$m. The applied voltage was adjusted so that the incident current density was the same for both structures. Bulk resistivities were used for the Cu (1.7 $\mu\Omega \cdot$ cm), and CoFe and NiFe (both 17 $\mu\Omega \cdot$ cm). Figures 5(b) and 5(c) show the total current density throughout the structure as a color plot for Cu and $CuN_x$ devices, respectively. The only difference between these simulations is the Cu versus $CuN_x$ as the capping and SV interlayer layers. Since Cu has approximately one-tenth the resistivity of the adjacent CoFe and NiFe layers, much of the current is shunted laterally through the Cu layers when the current is injected from the top point contact. On the other hand, $CuN_x$ has about the same resistivity of the CoFe and NiFe, which limits the current from easily spreading laterally. Thus, the useful current density in both CoFe fixed layer and NiFe free layer are kept higher with $CuN_x$ than with pure Cu.

Figure 6 shows the $J_x$ (lateral) and $J_z$ (normal to the layer interfaces) components of the calculated current density in the free layer, spacer layer, and the fixed layer for both types of devices. The current density injected from the nanocontact is 0.3 GA/cm$^2$, and is the same in both devices. In all layers, $J_z$ is greater in the $CuN_x$ devices under the nanocontact area. Additionally, $J_z$ in the $CuN_x$ does not depreciate as readily through the layers. The reduction of the free layer $J_z$ in Cu to that in $CuN_x$ is due to the initial spreading of current within the capping layer. To compare the longevity of $J_z$ through the device, we compare $J_z$ in the fixed layer to that in the free layer as a figure of merit analogous to a transmission coefficient. Thus, the transmission of useful current density is $J_z^{fixed}/J_z^{free}$, which we find to be 0.41 for Cu, and 0.74 for $CuN_x$ when we use the average current densities under the 50 nm diameter nanocontact. The more dramatic reduction of $J_z^{fixed}/J_z^{free}$ for the Cu devices is due to the spreading out of the current in each layer, since this layer has an order of magnitude lower resistivity. This process is readily observable in the $J_x$ simulations, where the Cu spacer layer shows a large increase over the $CuN_x$ spacer (similar results in the capping layer are omitted for brevity).

Figure 7 shows $J_z/J_x$ in the free and fixed layers of both devices. This ratio tells us how much the current is deviating into the plane: large $J_z/J_x$ means the current is preferentially along the injection direction, and $J_z/J_x = 0$ means the current is entirely in the plane. We can reasonably use $J_z/J_x = 1$ to define a radius for the injected current. In fact, the point satisfying this condition is that for which the power from $J_z$ has fallen by one half ($J_x$ does not contribute to the spin transfer, so the power associated with $J_z$ is the only relevant quantity). These positions are noted in the figure by up arrows for the free layer, and down arrows for the fixed layer. The ratio of the fixed and free layer radii is relevant to quantifying spreading: $r_{fixed}/r_{free}$ is 2.2 for Cu and 1.9 for $CuN_x$. This corresponds to a 75% reduction in the effective current spreading for $CuN_x$ devices, relative to Cu. Comparing the average of the free and fixed layer effective radii defines an effective contact area for mediating spin transfer between these layers. $CuN_x$ has an effective contact area that is

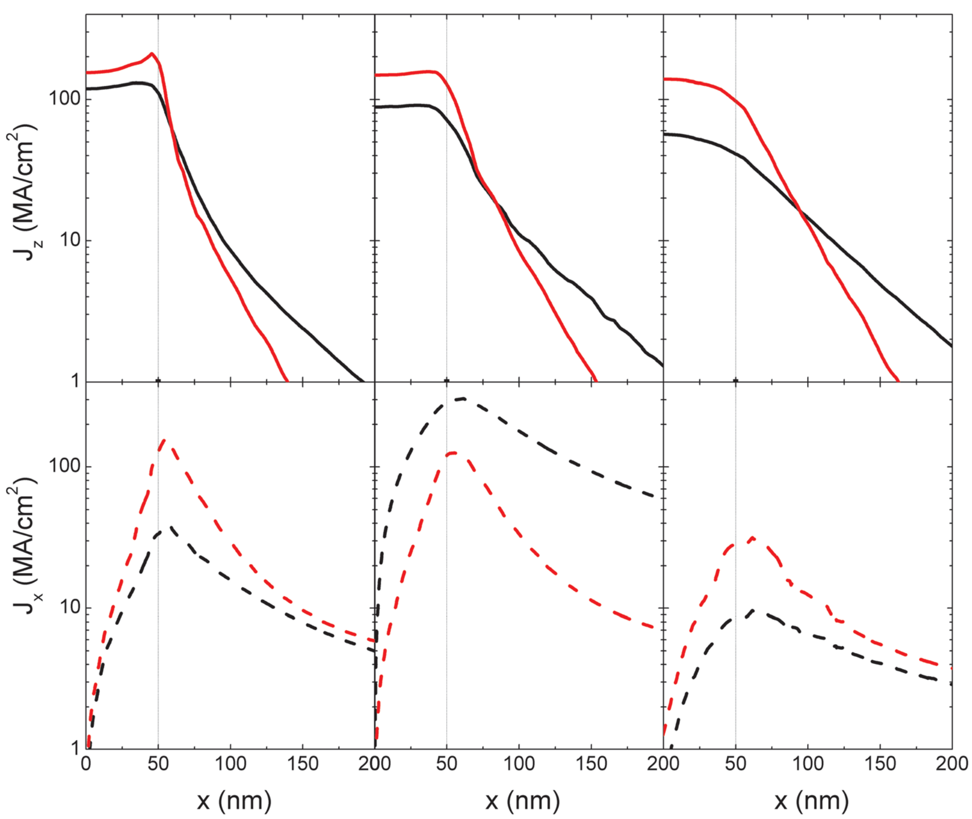


FIG. 6. Current densities in the $z$ and $x$ directions for the Cu (black) and $CuN_x$ (red) devices in the free (left), spacer (middle), and fixed (right) layers. In each layer, the $J_z$ is greater for the $CuN_x$ device, as a result of larger $J_x$ in the Cu device's cap (not shown) and spacer layers. The dashed lines indicate the radius of the nanocontact.

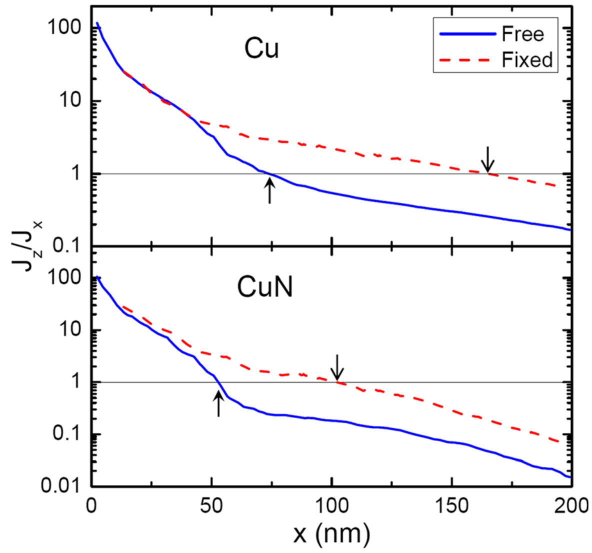


FIG. 7. $J_z/J_x$ as a function of lateral position gives an indication of how the current is spreading out in the plane. The position satisfying $J_z/J_x = 1$ is indicated by the arrows. This is the position of half power for $J_z$, which we used to define the effective contact radius, relative to the actual 50 nm nanocontact radius.

$(77.5/119.5)^2 = 42\%$ of that for Cu. This implies the $CuN_x$ device should have improved spin transfer between the free and fixed layers, which could lead to reductions in the onset current in STOs. These simulations can be considered boundaries for real devices, which in practice should have Cu interlayers to maximize the MR, while the capping layer that merges with the nanocontact should be the higher resistivity $CuN_x$ material.

## IV. CONCLUSIONS

In conclusion, we have shown that nitrification of Cu during the sputtering process may be advantageous for spintronics applications, such as spin transfer torque devices. The nitrogen content allows the electrical resistivity of $CuN_x$-based seed stacks to be tuned to nearly 20 times that of Cu-based stacks, while simultaneously reducing the surface roughness. CIP-MR values in test devices were maximized by incorporating the $CuN_x$ into the seed layer to assist planarization, and pure Cu for the spin-valve interlayer. Simulations of the current density in nanocontact-based spin torque oscillators suggest the use of $CuN_x$ rather than Cu can significantly increase the useful current density in spin transfer devices. The ability to reduce the effective contact area by as much as 42% may have significant impact on technologically relevant device characteristics, such as threshold current and the current required to reach high frequencies, power consumption, and device reliability.

## ACKNOWLEDGMENTS

The authors thank C. Bauer and D. Williams for help with the XRD. Support from The Swedish Foundation for Strategic Research (SSF), the Swedish Research Council (VR), the Göran Gustafsson Foundation, and the Knut and Alice Wallenberg Foundation is gratefully acknowledged. Johan Åkerman is a Royal Swedish Academy of Sciences Research Fellow supported by a grant from the Knut and Alice Wallenberg Foundation. Work performed at USF was supported by the National Science Foundation. The Center for Integrated Functional Materials is supported by the USAMRMC.

[1]M. N. Baibich, J. M. Broto, A. Fert, F. N. Van Dau, F. Petroff, P. Eitenne, G. Creuzet, A. Friederich, and J. Chazelas, Phys. Rev. Lett. **61**, 2472 (1988).
[2]G. Binasch, P. Grünberg, F. Saurenbach, and W. Zinn, Phys. Rev. B **39**, 4828 (1989).
[3]J. S. Moodera, J. Nassar, and G. Mathon, Annu. Rev. Mater. Sci. **29**, 381 (1999).
[4]J. S. Moodera, L. R. Kinder, T. M. Wong, and R. Meservey, Phys. Rev. Lett. **74**, 3273 (1995).
[5]T. Miyazaki and N. Tezuka, J. Magn. Magn. Mater. **139**, L231 (1995).
[6]J. Åkerman, Science **308**, 508 (2005).
[7]B. Engel, J. Åkerman, B. Butcher, R. Dave, M. DeHerrera, M. Durlam, G. Grynkewich, J. Janesky, S. Pietambaram, N. Rizzo *et al.*, IEEE Trans. Magn. **41**, 132 (2005).
[8]J. C. Slonczewski, J. Magn. Magn. Mater. **159**, L1 (1996).
[9]J. C. Slonczewski, J. Magn. Magn. Mater. **195**, L261 (1999).
[10]L. Berger, Phys. Rev. B **54**, 9353 (1996).
[11]D. Ralph and M. Stiles, J. Magn. Magn. Mater. **320**, 1190 (2008).
[12]M. Tsoi, A. G. M. Jansen, J. Bass, W.-C. Chiang, V. Tsoi, and P. Wyder, Nature **406**, 46 (2000).
[13]J. A. Katine, F. J. Albert, R. A. Buhrman, E. B. Myers, and D. C. Ralph, Phys. Rev. Lett. **84**, 3149 (2000).
[14]J. Grollier, V. Cros, A. Hamzic, J. M. George, H. Jaffrès, A. Fert, G. Faini, J. B. Youssef, and H. Legall, Appl. Phys. Lett. **78**, 3663 (2001).
[15]A. V. Nazarov, K. Nikolaev, Z. Gao, H. Cho, and D. Song, J. Appl. Phys. **103**, 07A503 (2008).
[16]D. Houssameddine, S. H. Florez, J. A. Katine, J.-P. Michel, U. Ebels, D. Mauri, O. Ozatay, B. Delaet, B. Viala, L. Folks *et al.*, Appl. Phys. Lett. **93**, 022505 (2008).
[17]A. M. Deac, A. Fukushima, H. Kubota, H. Maehara, Y. Suzuki, S. Yuasa, Y. Nagamine, K. Tsunekawa, D. D. Djayaprawira, and N. Watanabe, Nat. Phys. **4**, 803 (2008).
[18]T. Silva and W. Rippard, J. Magn. Magn. Mater. **320**, 1260 (2008).
[19]S. Bonetti, P. Muduli, F. Mancoff, and J. Åkerman, Appl. Phys. Lett. **94**, 102507 (2009).
[20]P. Muduli, Y. Pogoryelov, F. Mancoff, and J. Åkerman, IEEE Trans. Magn. **47**, 1575 (2011).
[21]W. H. Rippard, M. R. Pufall, S. Kaka, S. E. Russek, and T. J. Silva, Phys. Rev. Lett. **92**, 027201 (2004).
[22]S. Bonetti, V. Tiberkevich, G. Consolo, G. Finocchio, P. Muduli, F. Mancoff, A. Slavin, and J. Åkerman, Phys. Rev. Lett. **105**, 217204 (2010).
[23]F. B. Mancoff, N. D. Rizzo, B. N. Engel, and S. Tehrani, Appl. Phys. Lett. **88**, 112507 (2006).
[24]D. M. Borsa, S. Grachev, C. Presura, and D. O. Boerma, Appl. Phys. Lett. **80**, 1823 (2002).
[25]U. Hahn and W. Weber, Phys. Rev. B **53**, 12684 (1996).
[26]C. W. Miller, Z.-P. Li, J. Åkerman, and I. K. Schuller, Appl. Phys. Lett. **90**, 043513 (2007).
[27]C. W. Miller and D. D. Belyea, Appl. Phys. Lett. **96**, 022511 (2010).
[28]W. F. Egelhoff, Jr., R. D. McMichael, C. L. Dennis, M. D. Stiles, A. J. Shapiro, B. B. Maranville, and C. J. Powell, Appl. Phys. Lett. **88**, 162508 (2006).
[29]J. Moritz, F. Garcia, J. C. Toussaint, B. Dieny, and J. P. Nozieres, Europhys. Lett. **65**, 123 (2004).